Passive Sonar Ranging and Range-Doppler-Bearing Target Motion Analysis

Rémi Carloni Gertosio*, Gilles Gaonach*, Enzo Beyna*†, Liana Martin*†, Alexis Meyrat*†
*Thales Defense Mission Systems, 525 route des Dolines, BP 157, 06903 Sophia Antipolis Cedex, France
†École Navale, BCRM Brest, CC 600, 29240 Brest Cedex, France
Email: remi.carloni-gertosio@thalesgroup.com

***Abstract*—In passive sonar, target motion analysis (TMA) provides an estimate of the trajectory of a moving source, generally based on bearing and Doppler measurements. When the source presents a low bearing rate, the problem is ill-conditioned and difficult to solve without observer maneuver. To address this issue, we propose to estimate the instantaneous range of the source from its measured spectrum, using a conventional radiated ship noise model and a sound absorption model in seawater. The introduction of this new measurement in what becomes a range-Doppler-bearing TMA algorithm, ensures the uniqueness of the trajectory. Compared with standard Doppler-bearing TMA, convergence is faster and stability is improved, especially at low bearing rates.**

***Index Terms*—passive sonar, range estimation, ranging, target motion analysis, trajectory, tracking**

Notations: A vector is written in bold lowercase (e.g. $\mathbf{x}$) and a matrix in bold uppercase (e.g. $\mathbf{X}$). $\mathbf{x}_i$ and $\mathbf{X}_{ij}$ represent the ith and (i,j)th entry of $\mathbf{x}$ and $\mathbf{X}$, respectively. $\mathbf{X}_{i:}$ is a column vector formed by fixing the ith row of matrix $\mathbf{X}$. $\mathrm{diag}(\mathbf{x})$ is the diagonal matrix formed by the elements of its input. $\mathbf{X}^\top$ designates the transpose of $\mathbf{X}$. The overline (e.g. $\overline{\mathbf{x}}$) designates the true, i.e. noise-free, value of a measurement. The hat (e.g. $\hat{\mathbf{x}}$) designates the estimate of a value.

I. Introduction

Target motion analysis (TMA) provides valuable insight into the movement patterns and intentions of vessels in the marine environment, and therefore plays a pivotal role in a variety of applications such as navigation, collision avoidance and environmental monitoring.

In a plane with an orthonormal Cartesian coordinate system such as shown in Fig. 1, the coordinates $x_t(i)$ and $y_t(i)$ at time iT of a target with a uniform rectilinear motion are given by $x_t(i) = x_t(0) + iT\dot{x}_t$ and $y_t(i) = y_t(0) + iT\dot{y}_t$, where $\dot{x}_t$ and $\dot{y}_t$ are the target's velocity components, T is the observation period and $i \in [0 \ldots, I]$ is the time sample.

The most common passive sensor measurement is the target bearing. Denoting $(x_o(i), y_o(i))$ the observer's position at time iT, the true bearing $\overline{\beta}(i)$ verifies

$$\tan \overline{\beta}(i) = \frac{x_t(i) - x_o(i)}{y_t(i) - y_o(i)}. \tag{1}$$

In general, only a noisy measurement of the target bearing is known $\beta(i) = \overline{\beta}(i) + e_\beta(i)$ with $e_\beta(i)$ the bearing error term

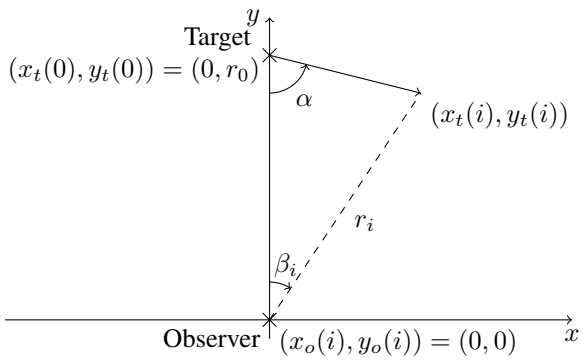

Fig. 1. Geometric setup. In the simulations, the observer is assumed to be fixed at the origin. The target, initially at a distance r_0 from the observer on the y-axis, has a route that forms an angle α with the y-axis, and has a velocity of 15 kn.

at time i. Substituting $\overline{\beta}(i)$ by $\beta(i)$ in Eq. (1) classically yields

$$\epsilon_\beta(i) = (x_t(i) - x_o(i)) \cos \beta(i) - (y_t(i) - y_o(i)) \sin \beta(i), \tag{2}$$

where $\epsilon_\beta(i) = -\overline{r_i} \tan e_\beta(i)$ represents the target location error due to bearing error and $\overline{r_i}$ the target instantaneous range.

Bearing-only TMA (BOTMA) recovers the target trajectory solely from bearing measurements. Its main weakness is the need for the observer to perform maneuvers to ensure the problem observability [1]. The addition of measurements of pure frequencies emitted by the target, such as those stemming from rotating engines, and more specifically their Doppler shift, removes this major limitation in what is known as Doppler-bearing TMA (DBTMA) [2].

A tonal ν of the target is seen by the observer at time i at frequency

$$\overline{f}(i) = \nu \left(1 - \frac{\dot{x}_t - \dot{x}_o(i)}{c} \sin \overline{\beta}(i) - \frac{\dot{y}_t - \dot{y}_o(i)}{c} \cos \overline{\beta}(i)\right), \tag{3}$$

with c the celerity of seawater and $(\dot{x}_o(i), \dot{y}_o(i))$ the observer's velocity components. The frequency measurement is likewise altered $f(i) = \overline{f}(i) + e_f(i)$, with $e_f(i)$ the frequency noise

term at time i. This leads to a target location error:

$$\epsilon_f(i) = iTc\Bigg(\frac{f(i)}{\nu} - \Bigg(1 - \frac{\dot{x}_t - \dot{x}_o(i)}{c}\sin\beta(i) - \frac{\dot{y}_t - \dot{y}_o(i)}{c}\cos\beta(i)\Bigg)\Bigg). \quad (4)$$

The TMA problem is commonly recast in a vector form. In the following, we shall consider only one frequency measurement for the sake of readability, noting that the framework lends itself to considering as many tonals as available. The unknown parameters are included in the parameter vector $\boldsymbol{\mu} = [1/\nu,\, x_t(0),\, \dot{x}_t,\, y_t(0),\, \dot{y}_t]^T$. Equations (2) and (4) up to a time I are embedded in an error vector

$$\boldsymbol{\epsilon} = [\epsilon_\beta(0), \epsilon_f(0), \epsilon_\beta(1), \epsilon_f(1) \ldots \epsilon_\beta(I), \epsilon_f(I)]^T \in \mathbb{R}^{2(I+1)}$$

which relates to the parameter vector $\boldsymbol{\mu}$ by

$$\boldsymbol{\epsilon} = \mathbf{A}\boldsymbol{\mu} - \mathbf{g}, \quad (5)$$

with the measurement vector

$$\mathbf{g} = \begin{bmatrix} x_o(0)c(0) - y_o(0)s(0) \\ 0 \\ x_o(1)c(1) - y_o(1)s(1) \\ T\left(c + \dot{x}_o(1)s(1) + \dot{y}_o(1)c(1)\right) \\ \vdots \\ x_o(I)c(I) - y_o(I)s(I) \\ IT\left(c + \dot{x}_o(I)s(I) + \dot{y}_o(I)c(I)\right) \end{bmatrix} \in \mathbb{R}^{2(I+1)}$$

where $c(i) = \cos\beta(i)$ and $s(i) = \sin\beta(i)$, and the measurement matrix

$$\mathbf{A} = \begin{bmatrix} 0 & c(0) & 0 & -s(0) & 0 \\ 0 & 0 & 0 & 0 & 0 \\ 0 & c(1) & Tc(1) & -s(1) & -Ts(1) \\ cTf(1) & 0 & Ts(1) & 0 & Tc(1) \\ \vdots & \vdots & \vdots & \vdots & \vdots \\ 0 & c(I) & ITc(I) & -s(I) & -ITs(I) \\ IcTf(I) & 0 & ITs(I) & 0 & ITc(I) \end{bmatrix}$$

which is of size $5 \times 2(I+1)$.

TMA is a challenging problem due to its highly nonlinear nature. Resolution techniques can be categorized into two families. The first, historic, family of algorithms involves recursive procedures, which are typically based on extended Kalman filters [3]. Numerous extensions have been proposed to improve convergence and accuracy performance. For example, a linearized version of the filter can be used to improve stability, but at the cost of a biased estimate [4]. More advanced filters, such as particle filters [5], have also been advocated. However, in practice, these methods tend to suffer from poor stability, which is inherent to their recursive nature and the variable observability of the problem.

The second family of algorithms builds upon the maximum likelihood estimator (MLE). In contrast to the recursive methods described above, the target parameters are estimated in a single pass using all measurements. The likelihood function is maximized with iterative optimization schemes, such as Newton-Gauss [6]. The main drawback of these methods is their potentially slow convergence. In this regard, it is essential to choose a suitable starting point. Moreover, the number of measurements and the tactical situation (i.e. observer and target position and trajectory) have an impact on the conditioning of the problem, and subsequently the convergence speed.

When the target bearing varies slowly, e.g. when the target is close to a collision course, the TMA problem is ill-conditioned, requiring more measurements or observer maneuvering. In this context, we propose to add an instantaneous range measurement to TMA, which should regularize and improve the observability of the problem. Once the bearing, Doppler and range measurements have been fused by TMA, the accuracy of the target localization should be improved compared with the sole initial range measurement.

The first contribution of this paper, which is developed in Section II, is to propose a passive sonar ranging algorithm based on the measurement of the noise power spectrum of a target, using a ship noise model and a sound absorption model in seawater. Passive sonar ranging algorithms usually include wavefront curvature measurements for sources within the near field of the antenna, triangulation techniques if there are two observers or more, and the analysis of multipath radiations if these exist and if the marine environment is known (sound speed profile, seabed) [7]. The proposed method operates in a more general case, irrespective of the target distance, the antenna size or the number of antennas.

The second contribution in Section III is the extension of the DBTMA framework to include an instantaneous range measurement, thus leading to a RDBTMA algorithm. This can come from the spectrum-based estimation presented in Section II or any other method. Research on TMA that incorporates range measurements is scarce compared to BOTMA and DBTMA. The observability of the range-only TMA problem is studied in [8]. Applications seem to concern only the passive radar domain, where the target range is obtained similarly by estimating absorption using a path loss law [9]. To our knowledge, the three measurements of bearing, Doppler and range have never been combined in a TMA algorithm.

II. Instantaneous passive range estimation

The ship noise and propagation models are first presented, after which the range estimator is constructed, and its performance evaluated on simulated data.

A. Models

1) Ship noise and propagation models: For the sake of readability, the overlines are omitted in this subsection. Ship noise is a combination of different contributions, notably from engines, propellers, water flow and cavitation effects. It is well characterized in the literature thanks to measurement

campaigns at sea [10]. A basic ship radiated noise model is a power law:

$$l_s(f) = l_{ref} - k \log_{10}\left(\frac{f}{f_{ref}}\right),$$

where $l_s(f)$ is the ship emission level in dB at $r_{ref} = 1$ m and frequency f, l_{ref} is the ship emission level in dB at range r_{ref} and frequency f_{ref}, and k is the power law coefficient. l_{ref} and k depend on the characteristics and the speed of the vessel, which are unknown.

Acoustic wave attenuation in the sea can be modeled at a range r by

$$20 \log_{10}\left(\frac{r}{r_{ref}}\right) + \alpha(f) r,$$

where the first term arises from spherical divergence losses and the second term from absorption in seawater. The volume absorption coefficient $\alpha(f)$ is commonly approached by a quadratic function [11]:

$$\alpha(f) = a_\alpha f^2 + b_\alpha f + c_\alpha,$$

with $a_\alpha = 8^{-9}$ $\mathrm{dB\,s^2\,km^{-1}}$, $b_\alpha = 3^{-5}$ $\mathrm{dB\,s\,km^{-1}}$ and $c_\alpha = 1.42\mathrm{e}{-2}$ $\mathrm{dB\,km^{-1}}$. We assume that the target noise measured by the observer comes from a direct path, which obviates the need to account for reflection losses on the seabed and surface.

Altogether, the power spectral density (PSD) of the received noise of a target l is written in decibels as follows:

$$l(f) = l_{ref} - k \log_{10}\left(\frac{f}{f_{ref}}\right) - 20 \log_{10}\left(\frac{r}{r_{ref}}\right) - \alpha(f) r. \tag{6}$$

Thereafter, let us note $p = 10^{l/10}$, the PSD in the linear scale.

2) Received ship noise PSD estimation: The acoustic signal measured by a sonar after beamforming in the direction of a target is the contribution of the noise of the latter target and the ambient noise of the sea. The broadband ship noise component is considered a random Gaussian signal with zero mean; it can be assumed stationary during the range measurement. Its PSD is estimated over N frequency channels of central frequencies $\{f_n\}_{n\in[1\dots N]}$ using Welch's method [12]. Let K be the number of segments used in Welch's method. We assume that the K segments are not overlapped. For the sake of simplicity, let us remove the PSD estimations at the zero and the Nyquist frequencies.

The PSD estimate, denoted $\{p_{ts}(f_n)\}_{n\in[1\dots N]}$, is a set of mutually independent random variables which are distributed as multiples of the chi-squared distribution with $2K$ degrees of freedom [13]. More particularly, their means are the true PSD $\{\overline{p_{ts}}(f_n)\}_{n\in[1\dots N]}$ and their variances are $\left\{\overline{p_{ts}}(f_n)^2/K\right\}_{n\in[1\dots N]}$.

The PSD of the background noise of the sea $\{\overline{p_s}(f_n)\}_{n\in[1\dots N]}$ is estimated similarly by pointing a beam in a source-free direction. It is also distributed as multiples of the chi-squared distribution.

Since ship noise and ambient sea noise are independent, the PSD of the received ship noise $\{\overline{p}(f_n)\}_{n\in[1\dots N]}$ verifies $\overline{p_{ts}}(f_n) = \overline{p}(f_n) + \overline{p_s}(f_n)$. It can therefore be estimated as $p(f_n) = p_{ts}(f_n) - p_s(f_n)$. $p(f_n)$ is the linear combination of two independent chi-squared distributions with the same degrees of freedom. To our knowledge, its probability density function has no analytic form. In practice, the number of segments K is large, allowing the use of the central limit theorem. $p(f_n)$ is therefore approximately Gaussian-distributed with mean $\overline{p}(f_n)$ and variance $(\overline{p_{ts}}(f_n)^2 + \overline{p_s}(f_n)^2)/K$.

B. Range estimation

1) Preliminaries: The PSD model (6) has three unknown parameters, namely l_{ref}, k and r, and is not linear in its parameters. We first propose the substitution of l_{ref} by $\xi = l_{ref} - 20 \log_{10}\left(\frac{r}{r_{ref}}\right)$ to make the model linear in its parameters. This change of variable is possible because the range is estimated instantaneously – in particular, measurements at different times are not aggregated to estimate the parameters.

Following the frequency discretization presented previously, the PSDs are arranged in N-sized vectors: $\mathbf{l}_n = l(f_n)$, $\mathbf{p}_n = p(f_n)$, $\mathbf{p_{ts}}_n = p_{ts}(f_n)$ and $\mathbf{p_s}_n = p_s(f_n)$. Equation (6) can now be expressed using the matrix formalism as:

$$\bar{\mathbf{l}} = \mathbf{C}\mathbf{x} \tag{7}$$

with $\mathbf{x} = [\xi, k, r]^T$ the parameters and $\mathbf{C} \in \mathbb{R}^{N\times 3}$ the model matrix, whose nth row is $\mathbf{C}_{n:} = [1, -\log_{10}\left(\frac{f_n}{f_{ref}}\right), -\alpha(f_n)]^\top$. In the linear scale, Eq. (7) writes $\overline{\mathbf{p}} = 10^{\mathbf{C}\mathbf{x}/10}$.

2) Maximum likelihood estimator: As the samples of $\mathbf{p}$ are independent, the negative log-likelihood function of $\mathbf{p}$ is asymptotically approximated by:

$$g_{\mathbf{p}}(\mathbf{x}) = \frac{K}{2} \sum_{n=1}^{N} \frac{\left(\mathbf{p}_n - 10^{\mathbf{C}_{n:}^T \mathbf{x}/10}\right)^2}{\overline{\mathbf{p_{ts}}}_n^2 + \overline{\mathbf{p_s}}_n^2} + \text{const.} \tag{8}$$

The maximum likelihood estimator, i.e. the maximum of $g_{\mathbf{p}}$, has no analytic form, requiring an iterative optimization algorithm to calculate it. We prefer to make a change of variable and consider the PSD in the logarithmic scale $\mathbf{l} = 10 \log_{10}(\mathbf{p})$. K is assumed large, therefore $|\mathbf{p}_n - \overline{\mathbf{p}}_n| \ll \overline{\mathbf{p}}_n$ and a Taylor expansion on the moments of $\mathbf{l}_n$ shows that it is of mean $\bar{\mathbf{l}}_n$ and of variance $\frac{1}{K}\left(\frac{10}{\log(10)}\right)^2 \frac{\overline{\mathbf{p_{ts}}}_n^2 + \overline{\mathbf{p_s}}_n^2}{\overline{\mathbf{p}}_n^2}$.

The central limit theorem is again used to approximate the negative log-likelihood function of $\mathbf{l}$:

$$\begin{aligned} g_{\mathbf{l}}(\mathbf{x}) &= \frac{K}{2}\left(\frac{\log(10)}{10}\right)^2 \sum_{n=1}^{N} \frac{\overline{\mathbf{p}}_n^2}{\overline{\mathbf{p_{ts}}}_n^2 + \overline{\mathbf{p_s}}_n^2} \left(\mathbf{l}_n - \mathbf{C}_{n:}^T \mathbf{x}\right)^2 + \text{const.} \\ &= \frac{K}{2}\left(\frac{\log(10)}{10}\right)^2 \| \operatorname{diag}(\overline{\mathbf{w}}) \odot (\mathbf{l} - \mathbf{C}\mathbf{x}) \|_2^2 + \text{const.}, \end{aligned} \tag{9}$$

where $\overline{\mathbf{w}}$ is a weighing vector such as $\overline{\mathbf{w}}_n^2 = \overline{\mathbf{p}}_n^2 / (\overline{\mathbf{p_{ts}}}_n^2 + \overline{\mathbf{p_s}}_n^2)$.

Therefore, the problem reduces to a weighted least squares. The weights are not known since the true PSDs are unknown; we propose to replace the latter by their measured versions,

noting that they do tend to the true PSDs when K is large. The estimate of $\mathbf{x}$ is then

$$\hat{\mathbf{x}} = \left(\mathbf{C}^T \operatorname{diag}(\mathbf{w})^2 \mathbf{C}\right)^{-1} \mathbf{C}^T \operatorname{diag}(\mathbf{w})^2 \mathbf{l}, \tag{10}$$

from which the range can be derived $\hat{r} = \hat{\mathbf{x}}_3$.

3) Variance estimate: For the purpose of RDBTMA, it is essential to provide an estimate of the variance of the range estimator $\hat{r}$. Eq. (8) gives the asymptotic approximation of the measurement likelihood; the related Fisher information matrix is

$$\mathbf{M} = K \left(\frac{\log(10)}{10}\right)^2 \mathbf{C}^T \operatorname{diag}(\overline{\mathbf{w}})^2 \mathbf{C}. \tag{11}$$

By replacing the weighing vector $\overline{\mathbf{w}}$ in $\mathbf{M}$ by $\mathbf{w}$, i.e. using the measured PSDs, a variance estimator is derived by $\hat{\sigma}^2_{\hat{r}} = [\mathbf{M}^{-1}]_{33}$. Note that it is not the Cramér-Rao lower bound (CRLB) of the estimator $\hat{r}$, as it is the result of an approximate likehood. Its validity shall be assessed in simulations.

C. Monte Carlo experiments

1) Simulation setup: Ship noise and background sea noise are simulated by filtering white Gaussian noise realizations with the PSD models of Eq. (6) for ship noise and Wenz model for sea noise [14]. The simulated PSDs are derived with Welch's method. Let us define the signal-to-noise ratio as the energy ratio in the sonar band between the target noise and the sea noise – it is a more meaningful way of fixing l_{ref}. Figure 2 shows examples of simulated PSDs in different configurations.

2) Hyperparameter choice: The method has two hyperparameters, both related to Welch's method, namely the number of frequency points N and the number of segments K. These must be set according to the desired integration time $t_{int} = KN/f_s$, with f_s the sonar sampling frequency.

Figure 3 shows the root mean squared error (RMSE) of the range estimate as a function of t_{int} for different couples (K, N). As it can be expected, at constant N, increasing K or, equivalently, the observation time, reduces the RMSE. More interestingly, for a fixed observation time, a higher number of segments K is preferable; this is due to the assumption of a large K underlying the range estimator. Note, however, that N must be large enough to ensure that there are enough frequency channels in which the target PSD is predominant, which explains the performance stall for $N = 32$.

3) Performances: The convergence of the estimator with t_{int} is first verified in Fig. 4. The RMSE does converge to zero, and the closer the target, the faster it converges (Fig. 4a). Moreover, as shown in Fig. 4b, the standard deviation error dominates the RMSE compared to the bias error, and this is all the more true the longer the integration time. In all subsequent experiments, t_{int} will be sufficiently large for the RMSE to be dominated by the standard deviation. Finally, the standard deviation estimator of $\hat{r}$ is biased, but close enough (below 30% in the considered cases) to be included in RDBTMA.

Figure 5 shows the accuracy of the target range estimate as a function of the actual range for different noise levels. The curves are displayed provided the problem is sufficiently well conditioned ($\operatorname{cond}(\mathbf{C}^T \operatorname{diag}(\mathbf{w})^2 \mathbf{C}) \leq$ 1e10). As expected, the closer the target, the more accurate the range estimate. In the low-noise cases, a degradation of the estimate is noted when the target is too close. Indeed, in this case, sound absorption in water is low, and range estimation, which relies on this effect, can be more difficult. Finally, the estimation of $\hat{\sigma}_{\hat{r}}$ is rather coarse, but still satisfactory. Except in poorly conditioned cases (SNR of 0 dB or high ranges), the deviation is limited to less than 30%.

III. Range-Doppler-bearing tracking

A. Model

The range estimate, even if relatively imprecise, becomes a valuable measurement when fused with bearing and Doppler measurements in TMA. Following the TMA framework presented in Section I, the target range estimate $r(i) = \overline{r}(i) + e_r(i)$ at time i verifies:

$$\epsilon_r(i) = (x_t(i) - x_o(i)) \sin\beta(i) + (y_t(i) - y_o(i)) \cos\beta(i) - r(i), \tag{12}$$

with $\epsilon_r(i) = e_r(i)$ the target location error due to the range estimation error.

The proposed new error vector is

$$\boldsymbol{\epsilon} = [\epsilon_\beta(0), \epsilon_f(0), \epsilon_r(0), \epsilon_\beta(1), \epsilon_f(1), \epsilon_r(1), \dots \\ \epsilon_\beta(I), \epsilon_f(I), \epsilon_r(I)]^T \in \mathbb{R}^{3(I+1)}$$

and the TMA model still writes $\boldsymbol{\epsilon} = \mathbf{A}\boldsymbol{\mu} - \mathbf{g}$ with the same parameter vector $\boldsymbol{\mu}$, the new measurement vector

$$\mathbf{g} = \begin{bmatrix} x_o(0)c(0) - y_o(0)s(0) \\ 0 \\ x_o(0)s(0) + y_o(0)c(0) + r(0) \\ x_o(1)c(1) - y_o(1)s(1) \\ T\left(c + \dot{x}_o(1)s(1) + \dot{y}_o(1)c(1)\right) \\ x_o(1)s(1) + y_o(1)c(1) + r(1) \\ \vdots \\ x_o(I)c(I) - y_o(I)s(I) \\ IT\left(c + \dot{x}_o(I)s(I) + \dot{y}_o(I)c(I)\right) \\ x_o(I)s(I) + y_o(I)c(I) + r(I) \end{bmatrix} \in \mathbb{R}^{3(I+1)},$$

and the new measurement matrix

$$\mathbf{A} = \begin{bmatrix} 0 & c(0) & 0 & -s(0) & 0 \\ 0 & 0 & 0 & 0 & 0 \\ 0 & s(0) & 0 & c(0) & 0 \\ 0 & c(1) & Tc(1) & -s(1) & -Ts(1) \\ cTf(1) & 0 & Ts(1) & 0 & Tc(1) \\ 0 & s(1) & Ts(1) & c(1) & Tc(1) \\ \vdots & \vdots & \vdots & \vdots & \vdots \\ 0 & c(I) & ITc(I) & -s(I) & -ITs(I) \\ IcTf(I) & 0 & ITs(I) & 0 & ITc(I) \\ 0 & s(I) & ITs(I) & c(I) & ITc(I) \end{bmatrix},$$

which is of size $5 \times 3(I+1)$.

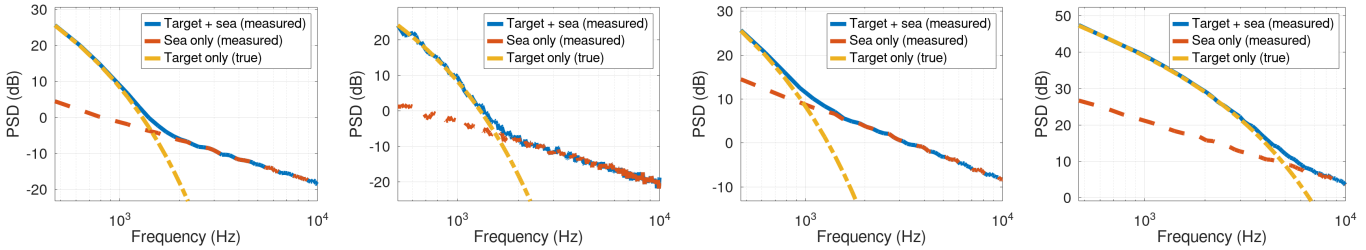

(a) $K = 1000$, $r = 5000$ m and SNR $= 40$ dB (b) $K = 62$, $r = 5000$ m and SNR $= 40$ dB (c) $K = 1000$, $r = 5000$ m and SNR $= 20$ dB (d) $K = 1000$, $r = 500$ m and SNR $= 40$ dB

Fig. 2. Example of simulated PSDs for $f_s = 20$ kHz, $t_{int} = 3.2$ s, $k = 19$ dB/decade.

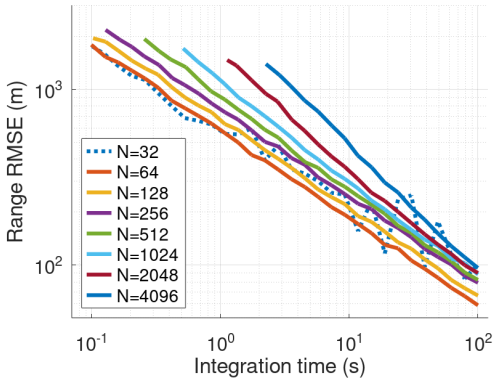

Fig. 3. RMSE of the estimated range as a function of t_{int} for different frequency point numbers N ($r = 5$ km, $f_s = 20$ kHz, SNR $= 40$ dB, $k = 19$ dB/decade, estimated over 1000 noise realizations).

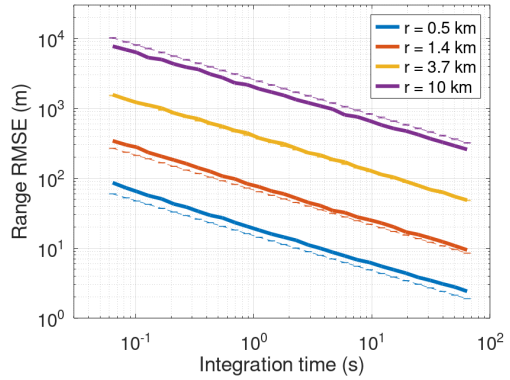

(a) Solid line: RMSE of $\hat{r}$. Dashed line: $\hat{\sigma}_{\hat{r}}$. The error bars, which are very small, indicate the standard deviation of $\hat{\sigma}_{\hat{r}}$.

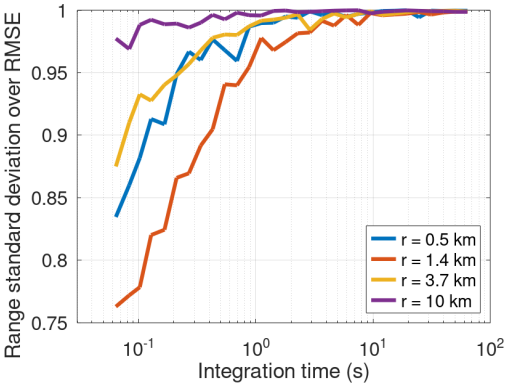

(b) Standard deviation over RMSE of $\hat{r}$. Note that the standard deviation is the one derived from the Monte Carlo experiments, not its estimation $\hat{\sigma}_{\hat{r}}$.

Fig. 4. Performance of the range estimator as a function of t_{int} for different ranges ($N = 128$, $f_s = 20$ kHz, SNR $= 40$ dB, $k = 19$ dB/decade, estimated over 1000 noise realizations).

B. Estimator

In this paper, we use and adapt the DBTMA algorithm proposed by Ho and Chan [15], part of the MLE family, which is interesting because it dispenses with an iterative minimization process, avoiding the problems of initial point choice and convergence, while bearing overall good performance.

Let $\mathbf{A_u} = [\mathbf{A}, -\mathbf{g}]$ be an augmented measurement matrix and $\boldsymbol{\mu_u} = [\boldsymbol{\mu}, 1]^T$ be an augmented solution vector. The TMA model now writes $\mathbf{A_u}\boldsymbol{\mu_u} = \boldsymbol{\epsilon}$.

If the bearing measurement errors are small, then $\cos\beta_i \approx \cos\overline{\beta}_i - e_\beta(i)\sin\overline{\beta}_i$ and $\sin\beta_i \approx \sin\overline{\beta}i + e_\beta(i)\cos\overline{\beta}_i$, such that the augmented measurement matrix $\mathbf{A_u}$ can be decomposed as

$$\mathbf{A_u} = \overline{\mathbf{A_u}} + \widetilde{\mathbf{A_u}}, \tag{13}$$

where $\overline{\mathbf{A_u}}$ is $\mathbf{A_u}$ with the noise-free measurements $\left\{\left(\overline{\beta}_i, \overline{f}_i, \overline{r}_i\right)\right\}_{i\in[0\ldots I]}$ and $\widetilde{\mathbf{A_u}}$ is the component due to the measurement noise:

$$\widetilde{\mathbf{A_u}} = \begin{bmatrix} 0 & e_\beta(0)\,\overline{\mathbf{u_\beta}}(0)^T \\ e_f(0) & e_\beta(0)\,\overline{\mathbf{u_f}}(0)^T \\ 0 & e_\beta(0)\,\overline{\mathbf{u_r}}(0)^T - e_r(0)\mathbf{v_r}^T \\ \vdots & \vdots \\ 0 & e_\beta(I)\,\overline{\mathbf{u_\beta}}(I)^T \\ e_f(I) & e_\beta(I)\,\overline{\mathbf{u_f}}(I)^T \\ 0 & e_\beta(I)\,\overline{\mathbf{u_r}}(I)^T - e_r(I)\mathbf{v_r}^T \end{bmatrix},$$

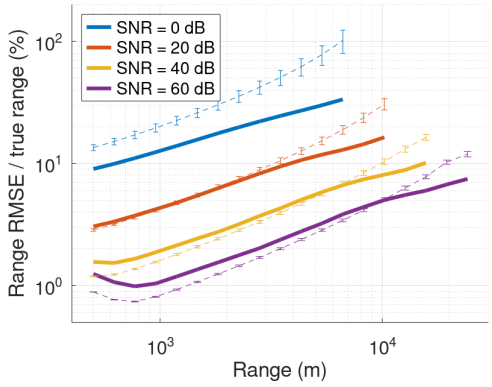

Fig. 5. RMSE of the estimated range over the true range as a function of the range for different SNRs ($K = 1000$, $N = 128$, $t_{int} = 6.4$ s, $k = 19$ dB/decade, estimated over 1000 noise realizations). Solid line: RMSE of $\hat{r}/r$, dashed line: $\hat{\sigma}_{\hat{r}}/r$, the error bars indicate the standard deviation.

with $\mathbf{v_r} = [0, 0, 0, 0, 1]^T$ and

$$\overline{\mathbf{u_\beta}}(i) = [-\sin\overline{\beta}_i, -iT\sin\overline{\beta}_i, -\cos\overline{\beta}_i, -iT\cos\overline{\beta}_i, x_o(i)\sin\overline{\beta}_i + y_o(i)\cos\overline{\beta}_i]^T,$$

$$\overline{\mathbf{u_f}}(i) = [0, iT\cos\overline{\beta}_i, 0, -iT\sin\overline{\beta}_i, iT\left(\dot{y}_o(i)\sin\overline{\beta}_i - \dot{x}_o(i)\cos\overline{\beta}_i\right)]^T,$$

$$\overline{\mathbf{u_r}}(i) = [\cos\overline{\beta}_i, iT\cos\overline{\beta}_i, -\sin\overline{\beta}_i, -iT\sin\overline{\beta}_i, -x_o(i)\cos\overline{\beta}_i + y_o(i)\sin\overline{\beta}_i]^T.$$

Let $\mathbf{R} = {\mathbf{A_u}}^T\mathbf{A_u}$ and

$$\begin{aligned}\mathbf{W} &= \mathbb{E}\left[\widetilde{\mathbf{A_u}}^T\widetilde{\mathbf{A_u}}\right] \\ &= \begin{bmatrix}0 & \mathbf{0} \\ \mathbf{0} & \sigma_\beta^2\sum_{i=0}^{I}\overline{\mathbf{u_\beta}}(i)\overline{\mathbf{u_\beta}}(i)^T\end{bmatrix} \\ &+ \begin{bmatrix}(Tc)^2\sigma_f^2\sum_{i=0}^{I}i^2 & \mathbf{0} \\ \mathbf{0} & \sigma_\beta^2\sum_{i=0}^{I}\overline{\mathbf{u_f}}(i)\overline{\mathbf{u_f}}(i)^T\end{bmatrix} \\ &+ \begin{bmatrix}0 & \mathbf{0} \\ \mathbf{0} & \sigma_\beta^2\sum_{i=0}^{I}\overline{\mathbf{u_r}}(i)\overline{\mathbf{u_r}}(i)^T + \sigma_r^2\mathbf{v_r}{\mathbf{v_r}}^T\end{bmatrix}.\end{aligned}$$

As proposed in [15], the true bearings in $\mathbf{W}$, which are unknown, are replaced by their noisy measurements. The TMA solution is estimated by minimizing the measurement error $\|\boldsymbol{\epsilon}\|^2 = {\boldsymbol{\mu_u}}^T\mathbf{R}\boldsymbol{\mu_u}$:

$$\underset{\boldsymbol{\mu_u}}{\operatorname{argmin}}\ {\boldsymbol{\mu_u}}^T\mathbf{R}\boldsymbol{\mu_u} \text{ such that } {\boldsymbol{\mu_u}}^T\mathbf{W}\boldsymbol{\mu_u} = 1. \quad (14)$$

Indeed, if the number of measurements I is large, then $\|\boldsymbol{\epsilon}\|^2 \approx {\boldsymbol{\mu_u}}^T\overline{\mathbf{A_u}}^T\overline{\mathbf{A_u}}\boldsymbol{\mu_u} + {\boldsymbol{\mu_u}}^T\mathbf{W}\boldsymbol{\mu_u}$. Minimizing the error under the given constraint amounts to minimizing asymptotically ${\boldsymbol{\mu_u}}^T\overline{\mathbf{A_u}}^T\overline{\mathbf{A_u}}\boldsymbol{\mu_u}$, which yields the true solution. The more rigorous proof showing that the derived estimator is asymptotically unbiased is similar to that given in [15].

The Lagrange multiplier method is employed to solve the constraint minimization. An auxiliary cost function is formed $(\boldsymbol{\mu_u}, \lambda) \mapsto {\boldsymbol{\mu_u}}^T\mathbf{R}\boldsymbol{\mu_u} + \lambda({\boldsymbol{\mu_u}}^T\mathbf{W}\boldsymbol{\mu_u} - 1)$, and the problem then amounts to solving

$$\mathbf{R}\boldsymbol{\mu_u} = \lambda\mathbf{W}\boldsymbol{\mu_u}, \quad (15)$$

which is none other than a generalized eigenvalue decomposition problem. Multiplying Eq. (15) on the left by $\boldsymbol{\mu_u}^T$ gives λ, so the sought-after solution is the eigenvector associated with the smallest eigenvalue. The solution vector of Eq. (14) is finally given by $\boldsymbol{\mu}_j = \boldsymbol{\mu}_{\mathbf{u}j}/\boldsymbol{\mu}_{\mathbf{u}6}$, $j \in [1 \ldots 5]$.

Cramér-Rao lower bound: Under the assumption that the bearing, Doppler and range measurement noises are zero mean Gaussian random variables of variance σ_β^2, σ_f^2 and σ_r^2 respectively, and mutually independent, the Fisher matrix of the RDBTMA problem is:

$$\mathbf{I_F} = \frac{1}{\sigma_\beta^2}\frac{\partial\boldsymbol{\beta}^T}{\partial\boldsymbol{\mu}}\frac{\partial\boldsymbol{\beta}}{\partial\boldsymbol{\mu}^T} + \frac{1}{\sigma_f^2}\frac{\partial\mathbf{f}^T}{\partial\boldsymbol{\mu}}\frac{\partial\mathbf{f}}{\partial\boldsymbol{\mu}^T} + \frac{1}{\sigma_r^2}\frac{\partial\mathbf{r}^T}{\partial\boldsymbol{\mu}}\frac{\partial\mathbf{r}}{\partial\boldsymbol{\mu}^T}, \quad (16)$$

from which the CRLB is derived.

C. Monte Carlo experiments

1) Simulation setup: The simulation setup is shown in Fig. 1. The trajectory angle α is related to the target bearing rate; when $\alpha = 0°$, the bearing rate is null and the trajectory is a collision course, while for $\alpha = 90°$ the bearing rate is maximum. Measurements are taken at a time period noted t_{int} during an observation time t_{obs}. The bearing and Doppler measurements are simulated with the addition of Gaussian noise of standard deviation 1% to comply with the low-noise assumption of the resolution method.

2) Performances: First, let us evaluate the addition of a distance measurement that strictly respects the assumptions made on the measurements (unbiased and low noise); therefore, in this experiment only, the range measurements are simulated with the addition of Gaussian noise of standard deviation 1% and do not come from the method of Section II. The RMSEs of the target trajectory parameters are shown in Fig. 6. The trends are consistent, as the estimates are more accurate for longer observation times. RDBTMA produces results that can be exploited very quickly, in around twenty seconds as opposed to several minutes for DBTMA.

RDBTMA is then evaluated as a function of the initial target distance, see Fig. 7. The fusion of range measurements with bearing and Doppler measurements results in a gain in ranging accuracy of at least 50% compared to the initial range measurements. Moreover, DBTMA takes five times longer to obtain a ranging accuracy similar to RDBTMA.

Robustness to small bearing rates is tested in Fig. 8 by varying the angle of the target trajectory α. The proposed method is unaffected by the bearing rate, with an initial distance estimation accuracy of the order of 2% within one minute of observation. In the absence of bearing rate, and more particularly in the case of a collision course, DBTMA does not find the solution as the problem is not observable. The threshold angle from which the estimate is similar to RDBTMA depends on the observation time. For example, after

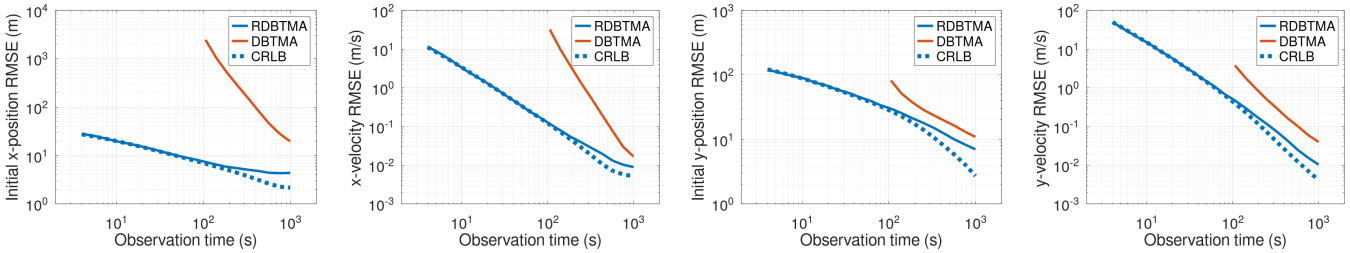

Fig. 6. RMSEs of the target trajectory parameters as a function of t_{obs} ($t_{int} = 1$ s, $r_0 = 5$ km, $\alpha = 45°$, target velocity of 15 kn $= 7.7$ m/s, estimated over 1000 noise realizations). It is noted that the range measurements are simulated here with the addition of Gaussian noise of standard deviation 1%. The CRLB is the one of RDBTMA. The results of DBTMA before $t_{obs} = 100$ s are not shown because they are particularly poor.

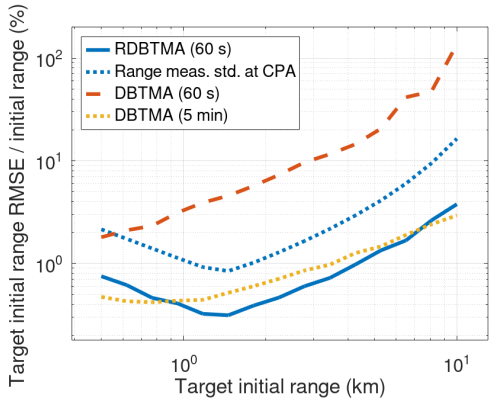

Fig. 7. RMSE of the target initial range estimate over the true initial range $\hat{r}_0/r_0$ as a function of the initial range r_0 for different t_{obs} ($t_{int} = 1$ s, $\alpha = 90°$, target velocity of 15 kn $= 7.7$ m/s, estimated over 250 noise realizations). The range measurements for RDBTMA come from the method presented in Section II ($K = 156$, $N = 128$, SNR $= 62$ dB at $r = 1$ km, $k = 19$ dB/decade). The blue dotted line is the standard deviation of the range measurement at the closest point of approach.

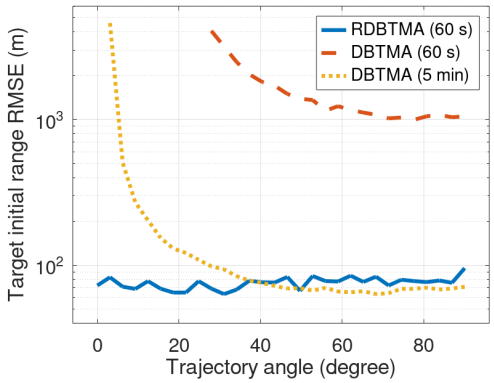

Fig. 8. RMSE of the target initial range estimate $\hat{r}_0$ as a function of the target's route angle α for different t_{obs} ($t_{int} = 1$ s, $r_0 = 5$ km, target velocity of 15 kn $= 7.7$ m/s, estimated over 1000 noise realizations). The range measurements for RDBTMA come from the method presented in Section II ($K = 625$, $N = 32$, SNR $= 62$ dB at $r = 1$ km, $k = 19$ dB/decade).

five minutes of observation, DBTMA performs similarly only for $\alpha \geq 30°$.

IV. Conclusion

A passive ranging method, based on the measurement of a ship radiated power spectrum, is proposed and included in a range-Doppler-bearing TMA framework. The range estimator is tested in various cases and generally provides operationally interesting ranges up to a few kilometers, depending on the signal-to-noise ratio. The addition of a range measurement to TMA, even if not very accurate, makes the problem better conditioned. Compared with conventional DBTMA, convergence times are drastically reduced. In addition, the case of collision courses, which was not observable without observer maneuver, is now observable.

Future work will focus on improving the modeling of ship radiated noise, to take account of tonals for example, as well as assessing the impact of propagation modeling, in the case of multipath radiations for instance.

References

[1] S. C. Nardone and V. J. Aidala, "Observability criteria for bearings-only target motion analysis," *IEEE Transactions on Aerospace and Electronic Systems*, vol. AES-17, no. 2, pp. 162–166, 1981.

[2] J. Passerieux, D. Pillon, P. Blanc-Benon, and C. Jauffret, "Target motion analysis with bearings and frequencies measurements via instrumental variable estimator (passive sonar)," in *International Conference on Acoustics, Speech, and Signal Processing,*, 1989, pp. 2645–2648 vol.4.

[3] V. Aidala and S. Hammel, "Utilization of modified polar coordinates for bearings-only tracking," *IEEE Transactions on Automatic Control*, vol. 28, no. 3, pp. 283–294, 1983.

[4] V. J. Aidala and S. C. Nardone, "Biased estimation properties of the pseudolinear tracking filter," *IEEE Transactions on Aerospace and Electronic Systems*, vol. AES-18, no. 4, pp. 432–441, 1982.

[5] S. M. Arulampalam, B. Ristic, N. Gordon, and T. Mansell, "Bearings-only tracking of manoeuvring targets using particle filters," *EURASIP Journal on Advanced Signal Processing*, vol. 2004, no. 15, p. 2351–2365, 2004.

[6] S. Nardone, A. Lindgren, and K. Gong, "Fundamental properties and performance of conventional bearings-only target motion analysis," *IEEE Transactions on Automatic Control*, vol. 29, no. 9, pp. 775–787, 1984.

[7] A. D. Waite, "Passive sonar," in *Sonar for Practising Engineers, 3rd Edition*. Chichester: John Wiley & Sons Ltd, 2002, ch. 8, pp. 125–260.

[8] C. Jauffret, A.-C. Pérez, and D. Pillon, "Observability: Range-only versus bearings-only target motion analysis when the observer maneuvers

smoothly," *IEEE Transactions on Aerospace and Electronic Systems*, vol. 53, no. 6, pp. 2814–2832, 2017.

[9] G. Gu, "A novel power-bearing approach and asymptotically optimum estimator for target motion analysis," *IEEE Transactions on Signal Processing*, vol. 59, no. 3, pp. 912–922, 2011.

[10] S. C. Wales and R. M. Heitmeyer, "An ensemble source spectra model for merchant ship-radiated noise," *The Journal of the Acoustical Society of America*, vol. 111, no. 3, pp. 1211–1231, 03 2002.

[11] R. E. Francois and G. R. Garrison, "Sound absorption based on ocean measurements. Part II: Boric acid contribution and equation for total absorption," *The Journal of the Acoustical Society of America*, vol. 72, no. 6, pp. 1879–1890, 12 1982.

[12] P. Welch, "The use of fast Fourier transform for the estimation of power spectra: A method based on time averaging over short, modified periodograms," *IEEE Transactions on Audio and Electroacoustics*, vol. 15, no. 2, pp. 70–73, 1967.

[13] O. M. Solomon, Jr, "PSD computations using Welch's method," Sandia National Lab, Tech. Rep., 12 1991.

[14] G. M. Wenz, "Acoustic Ambient Noise in the Ocean: Spectra and Sources," *The Journal of the Acoustical Society of America*, vol. 34, no. 12, pp. 1936–1956, 12 1962.

[15] K. Ho and Y. Chan, "An asymptotically unbiased estimator for bearings-only and doppler-bearing target motion analysis," *IEEE Transactions on Signal Processing*, vol. 54, no. 3, pp. 809–822, 2006.